J Water Environ Nanotechnol 2026, 11(3): 405-419
10.22090/jwent.2025.2076178.1992

RESEARCH PAPER

Magnetic Quaternary Nanocomposites Integrate PANI, Graphene Oxide, Chitosan, and ZrO_2/ZnO to Synergistically Photodegrade Methylene Blue and Adsorb Cd^{2+}, Cr^{6+}, and Ni^{2+} From Wastewater

Ibrahim A.Kareem Al-Dulaimi[1], *Amer Al-Nafiey*[2*]

[1]Midland Refineries Company (MRC) / Daura Refineries, Baghdad, Iraq
[2]Department of Laser Physics, College of science for women, University of Babylon, Iraq

*Corresponding Author(s)
Email:
amer76z@yahoo.com

Article History:

Received: 2025-10-29
Revised: 2026-01-10
Accepted: 2026-01-20

How to cite this article
Al-Dulaimi Ia, Al-Nafiey A. Magnetic Quaternary Nanocomposites Integrate PANI, Graphene Oxide, Chitosan, and ZrO_2/ZnO to Synergistically Photodegrade Methylene Blue and Adsorb Cd^{2+}, Cr^{6+}, and Ni^{2+} from Wastewater. J Water Environ Nanotechnol 2026, 11(3): 405-419, DOI: 10.22090/jwent.2025.2076178.1992

HIGHLIGHTS

- Magnetic PANI/GO/Chitosan/ZrO_2-ZnO quaternary nanocomposites were synthesized.
- ZrO_2-based nanocomposite degraded ~95% of methylene blue within 48 h.
- Cd^{2+}, Cr^{6+}, and Ni^{2+} were removed, with up to 88% Cd^{2+} adsorption.
- Fe_3O_4 core enables simple magnetic separation and nanocomposite reuse.

ABSTRACT

This study reports the synthesis of magnetic quaternary nanocomposites based on polyaniline, graphene oxide, chitosan, Fe_3O_4, and metal oxides (ZrO_2 or ZnO) via an in-situ polymerization approach. The structural, optical, and morphological properties of the synthesized nanocomposites were investigated using UV–Vis spectroscopy, X-ray diffraction, and scanning electron microscopy. Quantitative XRD analysis confirmed the nanocrystalline nature of the composites, while SEM analysis revealed a porous morphology with particle sizes mainly in the range of 50–200 nm.

The photocatalytic performance was evaluated through methylene blue degradation under ambient laboratory light. The ZrO_2-based nanocomposite achieved approximately 95% degradation of methylene blue (50 ppm) after 48 h, while the ZnO-based system showed about 85% degradation under identical conditions. Heavy metal adsorption experiments analyzed by ICP-OES demonstrated effective removal of Cd^{2+}, Cr^{6+}, and Ni^{2+} ions, with removal efficiencies reaching up to 88% for Cd^{2+} and improved selectivity toward Cr^{6+} and Ni^{2+} in the ZrO_2-containing composite.

The results highlight the synergistic role of the quaternary structure in combining photocatalytic activity, adsorption capability, and magnetic recoverability within a single platform. These multifunctional nanocomposites show promise for integrated wastewater treatment applications involving both organic dyes and toxic metal ions.

KEYWORDS:

Polyaniline Nanocomposites; Photocatalysis; Heavy Metal Adsorption; Graphene Oxide; Magnetic Materials

©2026 The Author(s). Published by the Iranian Environmental Mutagen Society. This work is licensed under the Creative Commons Attribution 4.0 International License (CC BY 4.0). To view a copy of this license, visit http://creativecommons.org/licenses/by/4.0/.

INTRODUCTION

The increase in industrial activities has contributed to an increase in hazardous loading in the aquatic environment. In this regard, it is important to consider synthetic dyes and toxic heavy metals, such as cadmium (Cd), chromium (Cr), and nickel (Ni), as these contaminants disturb aquatic ecosystems when they persist in the environment for long periods of time, are toxic, and exhibit bioaccumulation potential in living organisms [1, 2]. Methylene blue (MB), for example, is a synthetic dye known for its use in the textile, printing, and pharmaceutical industries. The discharge of methylene blue in wastewater potentially can occur simultaneously with the same heavy metals that originated from electroplating, mining, and the chemical industries, which usually include cadmium, chromium, and nickel [3]. Conventional methods for treating wastewater include chemical precipitation, coagulation–flocculation, and membrane filtration and often have limitations, including low treatment efficacy, increased treatment costs, and the by-products (secondary waste). As a result, there have been a lot of new and innovative efforts in producing advanced, sustainable, and multifunctional materials for concurrent dye and heavy metal removal [4, 5].

On the other hand, nanotechnology may provide a unique opportunity for wastewater remediation processes due to the high surface area, tailored surface chemistry on nanomaterials, and improved reactivity [6]. Graphene oxide (GO) has abundant oxygenated functional groups and has a high surface area, allowing for strong interactions with organic dyes and metal cations through electrostatic forces, hydrogen bonding, and π–π stacking [7, 8].

Moreover, magnetic Fe_3O_4 nanoparticles are suitable for catalytic and adsorption processes due to their superior superparamagnetic properties, biocompatibility, and ease of recovery with magnetic force [9]. Metal oxides such as zirconium dioxide (ZrO_2) and zinc oxide (ZnO) improve photocatalytic activity, stability, and (re)usability [10, 11]. Plus, chitosan (CS), a naturally available biopolymer, can better adsorb metal ions in wastewater due to the additional amine and hydroxyl groups [12]. Conducting polymers, such as polyaniline (PANI), possess excellent adsorption ability due to their conjugated backbones and chemical stability, in addition to the potential to form strong interfacial interactions with other nanomaterials [13]. Selecting these properties from each component to integrate into a single quaternary nanocomposite would form a synergistic effect and create nanocomposites with higher adsorption ability, effective photocatalytic degradation, and easy recyclability for wastewater applications [14, 15].

In this study, we have synthesized and evaluated two multifunctional nanocomposites, PANI/Fe_3O_4–GO/CS–ZrO_2 and PANI/Fe_3O_4–GO/CS–ZnO. Each composite was carefully characterized using many spectroscopic and microscopic assessment techniques to demonstrate their structural, optical, and morphological properties. Their demonstrated adsorption and photocatalytic activity were analysed through methylene blue (MB) degradation and the elimination of Cd^{2+}, Cr^{6+}, and Ni^{2+} from aqueous solutions utilizing UV–Vis spectrophotometry and inductively coupled plasma optical emission spectroscopy (ICP-OES). This research aims to advance the development of environmentally friendly and magnetically recoverable nanocomposites for effective wastewater treatment.

EXPERIMENTAL

Materials and Chemicals

Graphene oxide (GO) and Fe_3O_4 nanoparticles were purchased from local Iraqi markets. Nano chitosan (Cs), zirconium oxide (ZrO_2), acetic acid, hydrochloric acid (HCl), aniline, ammonium persulfate (APS, $(NH_4)_2S_2O_8$), sodium alginate (SA), sodium dodecyl sulfate (SDS), ethanol (EtOH), and distilled water (DI) were used as received without further purification.

Synthesis of Fe_3O_4–GO Nanocomposite

The Fe_3O_4–GO nanocomposite was prepared using a simple impregnation method. Briefly, 0.15 g of graphene oxide (GO) was dispersed in 100 mL of distilled water and ultrasonicated for 30 min using a bath sonicator operating at room temperature (25 °C) to achieve complete exfoliation of GO sheets. The pH of the suspension was approximately neutral (pH ≈ 6.8) without further adjustment.

Subsequently, 0.15 g of Fe_3O_4 nanoparticles was gradually added to the GO suspension under continuous magnetic stirring. The mixture was further ultrasonicated for 30 min to ensure uniform impregnation of Fe_3O_4 nanoparticles onto the GO sheets. The resulting homogeneous Fe_3O_4–GO suspension was used directly for subsequent composite fabrication without additional drying or calcination steps.[9].

Synthesis of ZrO_2/Chitosan (CS–ZrO_2) Nanocomposite

Chitosan–zirconium dioxide (CS–ZrO_2) nanocomposite was synthesized via physical interaction and electrostatic binding. Initially, 0.5 g of chitosan nanoparticles was dissolved in 25 mL of 1% (v/v) acetic acid to obtain a 2% (w/v) chitosan solution under magnetic stirring at room temperature until complete dissolution. The solution pH was approximately 4.0–4.5.

Separately, 0.8 g of ZrO_2 nanoparticles was dispersed in the chitosan solution and ultrasonicated for 20 min to promote uniform dispersion. The suspension was then magnetically stirred at room temperature (25 °C) for 8 h to allow effective interaction between chitosan functional groups (–NH_2 and –OH) and ZrO_2 surfaces.

After completion, the composite was purified by repeated ultracentrifugation and washing with ultrapure water until neutral pH was reached, removing excess acetic acid and unbound chitosan. The final CS–ZrO_2 nanocomposite was dried at room temperature for 24 h and stored in a desiccator for further use [10].

Preparation of Fe_3O_4–GO/CS–ZrO_2 Hybrid Nanocomposite

The Fe_3O_4–GO/CS–ZrO_2 hybrid nanocomposite was prepared by combining the previously synthesized components. The CS–ZrO_2 suspension was slowly added to the Fe_3O_4–GO suspension under vigorous magnetic stirring and maintained for 1 h at room temperature to promote homogeneous mixing.

The resulting mixture was subsequently ultrasonicated for an additional 60 min to prevent aggregation and ensure uniform distribution of CS–ZrO_2 over the Fe_3O_4–GO framework. The obtained Fe_3O_4–GO/CS–ZrO_2 hybrid dispersion was directly used for in-situ polymerization of aniline.

Synthesis of PANI/Fe_3O_4–GO/CS–ZrO_2 Quaternary Nanocomposite

In-situ oxidative polymerization of aniline was employed to synthesize the final quaternary nanocomposite. The Fe_3O_4–GO/CS–ZrO_2 dispersion was first ultrasonicated for 30 min to ensure complete dispersion. Then, 1 mL of aniline monomer was dissolved in 30 mL of 1 M HCl and added dropwise to the dispersion under continuous stirring. The mixture was ultrasonicated for 2 h to enhance monomer adsorption onto the composite surface.

Polymerization was initiated by the slow addition of 2.5 g of ammonium persulfate (APS), previously dissolved in 40 mL of 1 M HCl, maintaining an APS/aniline molar ratio close to 1. The reaction was carried out under continuous stirring in an ice bath at 0–5 °C for 2–4 h to control polymer growth and prevent over-oxidation.

After polymerization, the dark green suspension was aged overnight at 4 °C to ensure complete polymer formation. The resulting PANI/Fe_3O_4–GO/CS–ZrO_2 nanocomposite was collected by filtration, washed repeatedly with distilled water and dilute HCl to remove unreacted monomer and oligomers, and finally dried in an oven at 80 °C for 10 h.

Photocatalytic Degradation of Methylene Blue

Photocatalytic degradation experiments were carried out using a conventional laboratory light source under continuous stirring to ensure homogeneous dispersion of the catalyst. In a typical experiment, 100 mL of methylene blue (MB) aqueous solution with initial concentrations of 50, 100, and 200 mg/L was transferred into a glass beaker. The catalyst dosage was fixed at 0.10 g for PANI/Fe_3O_4–GO/CS–ZrO_2 and 0.07 g for PANI/Fe_3O_4–GO/CS–ZnO.

Before light irradiation, the suspension was magnetically stirred and kept in a dark locker for approximately 2 h to establish adsorption–desorption equilibrium between MB molecules and the catalyst surface. Afterward, the suspension was exposed to laboratory ambient light while stirring at room temperature (25 °C). The distance between the light source and the solution was kept constant throughout the experiments.

At selected irradiation times, aliquots were withdrawn from the reaction mixture, and the catalyst was separated using magnetic decantation. The residual MB concentration was determined by measuring the absorbance at 664 nm using a UV–Vis spectrophotometer. The degradation performance was evaluated based on the decrease in absorbance intensity relative to the initial concentration.

Heavy Metal Adsorption Experiments

Batch adsorption experiments were conducted to evaluate the removal of Cd^{2+}, Cr^{6+}, and Ni^{2+} ions from aqueous solutions using the synthesized nanocomposites. In each experiment, 100 mL of single-metal aqueous solution with a known initial concentration was transferred into a beaker and treated with a fixed amount of the adsorbent.

The suspension was continuously stirred at room temperature (25 °C) to ensure uniform contact between the metal ions and the adsorbent surface. The solution pH was maintained at neutral conditions (pH ≈ 7) without further adjustment. After a predefined contact time, the adsorbent was separated from the solution by magnetic decantation.

The residual concentrations of Cd^{2+}, Cr^{6+}, and Ni^{2+} ions in the supernatant were quantified using inductively coupled plasma optical emission spectroscopy (ICP-OES). The adsorption performance was evaluated based on the reduction in metal ion concentration before and after treatment.

RESULTS AND DISCUSSION

UV–Vis Absorbance Spectrum

The UV–Vis absorbance spectrum of the synthesized PANI/Fe_3O_4–GO/CS–ZrO_2, PANI/Fe_3O_4–GO/CS–ZnO nanocomposite is presented in Fig. 1(A, B).

Fig. 1(A) shows the UV–Vis absorbance spectrum of the synthesized PANI/Fe_3O_4–GO/CS–ZrO_2 nanocomposite. The spectrum displays a broad and intense absorption band spanning the 200–1000 nm range, indicative of strong light-harvesting ability across the ultraviolet, visible, and near-infrared regions. A sharp peak centered on ~225 nm is attributed to π–π^* transitions in the benzenoid rings of polyaniline (PANI), confirming its successful integration into the hybrid matrix [11]. Additionally, a shoulder around ~280 nm likely corresponds to n–π^* transitions from quinoid units in PANI and oxygen-containing groups in graphene oxide (GO), which are known to contribute to the absorption in this region [12].

The prolonged absorption tail beyond 400 nm is

J Water Environ Nanotechnol, 2026, 11(3): 405-419
10.22090/jwent.2025.2076178.1992

characteristic of inorganic metal oxides like Fe_3O_4 and ZrO_2, suggesting their role in extending the optical activity of the nanocomposite due to scattering and interfacial charge transfer effects [13]. This broad absorption is advantageous in photocatalytic and photothermal processes by enabling better utilization of the solar spectrum [14]. Furthermore, the gradual decrease in absorbance at longer wavelengths is consistent with semiconducting nanostructures, indicating effective interfacial electronic interactions between PANI, GO, Fe_3O_4, and ZrO_2.

Fig. 1(B) illustrates the UV–Vis absorbance spectrum of the PANI/Fe_3O_4–GO/CS–ZnO nanocomposite. Similar to the previous sample, strong absorption is observed in the UV region, with considerable absorption extended into the visible domain. A distinct peak between 270–300 nm arises from π–π^* transitions in the conjugated C=C bonds of PANI and GO. A subtle shoulder near ~400 nm is likely caused by n–π^* transitions and possible charge transfer interactions between Fe_3O_4 and ZnO components, as previously reported in ternary or quaternary nanocomposite systems [15].

The decline in absorbance beyond 600 nm reflects reduced photon absorption at higher wavelengths, supporting the presence of indirect transitions commonly associated with ZnO-based and Fe_3O_4-based hybrid materials. This behaviour reinforces the material's potential in optoelectronic, photocatalytic, and solar energy conversion applications through synergistic enhancements in light absorption and charge separation.

The absorption coefficient (α) of the PANI/Fe_3O_4–GO/CS–ZrO_2, PANI/Fe_3O_4–GO/CS–ZnO nanocomposite is calculated from the absorbance data using the relation:

$$\alpha = 2.303 \times A / d \quad (1)$$

Where A is the absorbance and d is the optical path length (assumed to be 1 cm in this study). The resulting α values as a function of wavelength are plotted in Fig. 2(A, B).

Fig. 2(A) presents the absorption coefficient spectrum of the PANI/Fe_3O_4–GO/CS–ZrO_2 nanocomposite. The material

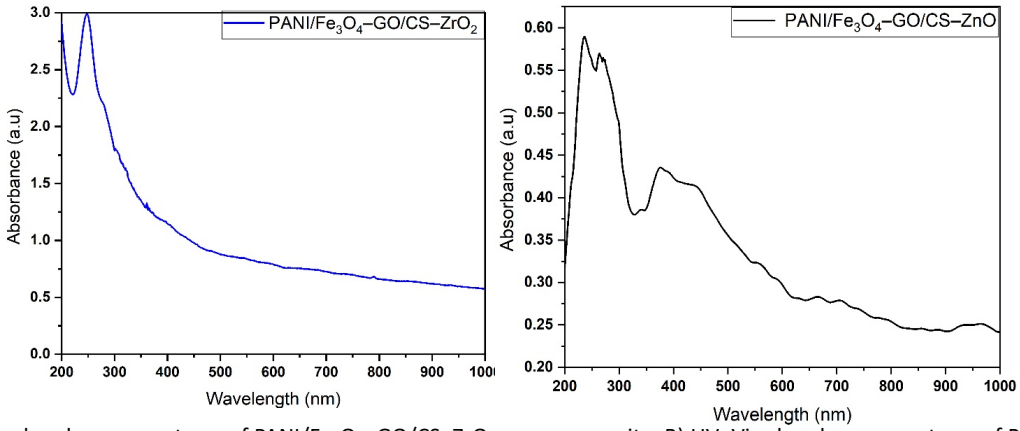

Fig. 1. A) UV–Vis absorbance spectrum of PANI/Fe_3O_4–GO/CS–ZrO_2 nanocomposite. B) UV–Vis absorbance spectrum of PANI/Fe_3O_4–GO/CS–ZnO nanocomposite

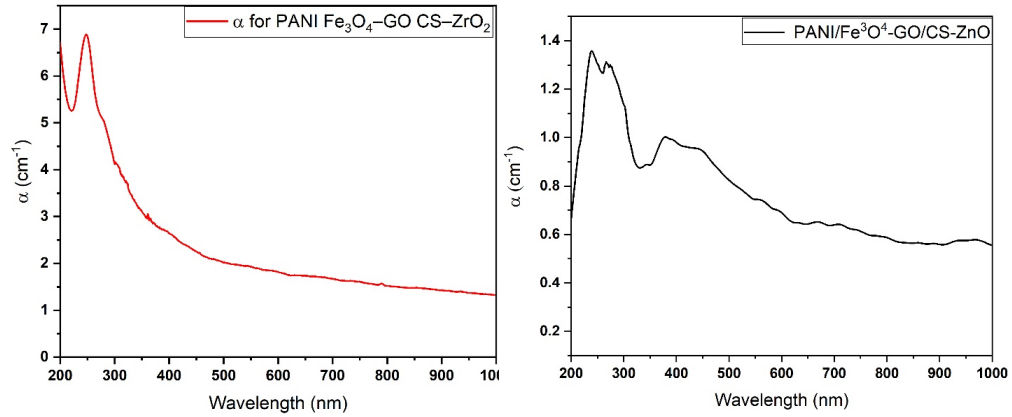

Fig. 2. Absorption coefficient (α) of the PANI/Fe_3O_4–GO/CS–ZrO_2 nanocomposite as a function of wavelength.

exhibits a high absorption coefficient in the ultraviolet (UV) region, with α values reaching approximately 6.8–7.0 cm^{-1} around 225–260 nm. This strong absorption is primarily attributed to π–π* electronic transitions in the conjugated polyaniline backbone, as well as transitions associated with GO and Fe_3O_4 components. As the wavelength increases, α gradually decreases, falling below 2 cm^{-1} in the near-infrared (NIR) region. This trend reflects a typical semiconducting behavior, indicating efficient absorption in the UV range and moderate absorption across the visible spectrum, which is advantageous for photocatalytic and optoelectronic applications.

Fig. 2(B) shows the absorption coefficient of the PANI/Fe_3O_4–GO/CS–ZnO nanocomposite. A pronounced absorption peak appears between 230–260 nm, corresponding to π–π* transitions of aromatic C=C bonds within the PANI and GO framework. A secondary shoulder between 280–300 nm is associated with n–π* transitions, likely originating from quinoid structures in PANI and oxygen-containing functional groups in GO [2]. The broader absorption in the 300–600 nm region suggests additional electronic transitions or interfacial charge transfer mechanisms involving Fe_3O_4 and ZnO phases. Beyond 600 nm, the steady decline in α indicates reduced photon absorption, consistent with materials exhibiting indirect or hybrid semiconductor behaviour.

Together, both spectra confirm the broad-spectrum light interaction of these nanocomposites, stemming from synergistic effects between the conjugated polymer matrix, conductive GO sheets, and semiconducting oxide nanoparticles. These features make the materials promising for applications in solar energy harvesting, photocatalysis, and photodetectors.

The transmittance spectrum of the PANI/Fe_3O_4–GO/CS–ZrO_2 and PANI/Fe_3O_4–GO/CS–ZnO nanocomposites is shown in Fig. 3(A) over the wavelength range of 200–1000 nm. Fig. 3(A) presents the transmittance spectrum of the PANI/Fe_3O_4–GO/CS–ZrO_2 nanocomposite over the wavelength range of 200–1000 nm. The material exhibits very low transmittance in the ultraviolet (UV) region, particularly below 400 nm, highlighting strong photon absorption. This behaviour is primarily attributed to π–π* electronic transitions in the aromatic structures of polyaniline (PANI), as well as interfacial charge transfer and electronic excitations involving the Fe_3O_4 and ZrO_2 phases. As the wavelength increases toward the visible and near-infrared (NIR) regions, the transmittance rises gradually, reaching approximately 0.27 (a.u.) at 1000 nm. This trend reflects a reduced optical absorption at longer wavelengths, characteristic of semiconducting hybrid nanostructures. The material's ability to strongly absorb UV light while permitting partial transmittance in the NIR supports its potential in solar shielding, optoelectronic devices, and photocatalytic applications.

Fig. 3(B) shows the transmittance spectrum of the PANI/Fe_3O_4–GO/CS–ZnO nanocomposite across the same spectral range. The composite also displays low transmittance in the UV range (200–350 nm), with a minimum value of approximately 0.26 (a.u.) near 270 nm. This strong absorption corresponds to π–π* transitions in PANI and GO, along with n–π* transitions and electronic transitions involving ZnO and Fe_3O_4 nanoparticles. Beyond 400 nm, the transmittance steadily increases, reaching a stable value around 0.55–0.58 (a.u). In the NIR region (>800 nm). This increase signifies the weakening of absorption at higher wavelengths, consistent with materials that possess indirect band gap behaviour. The observed optical properties confirm the nanocomposite's suitability for broad-spectrum light filtering, energy harvesting, and environmental remediation technologies.

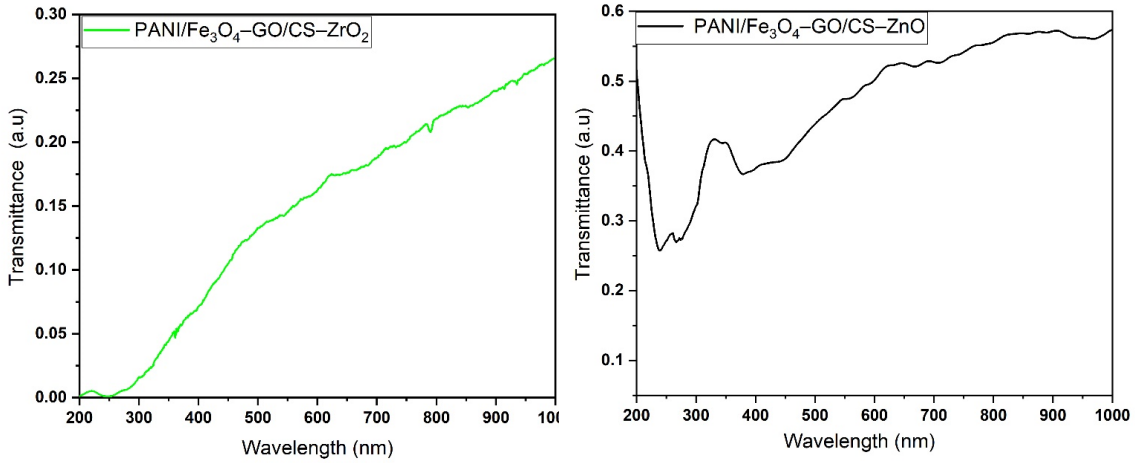

Fig. 3. A) Transmittance spectrum of the PANI/Fe_3O_4–GO/CS–ZrO_2 nanocomposite as a function of wavelength. B) Transmittance spectrum of the PANI/Fe_3O_4–GO/CS–ZnO nanocomposite

J Water Environ Nanotechnol, 2026, 11(3): 405-419
10.22090/jwent.2025.2076178.1992

The optical band gap (Eg) of the PANI/Fe_3O_4–GO/CS–ZrO_2, PANI/Fe_3O_4–GO/CS–ZnO nanocomposite was estimated using the Tauc plot method. The Tauc relation for a direct allowed transition is given by:

$$(\alpha h\nu)^2 = A(h\nu - Eg) \quad (2)$$

Where α is the absorption coefficient, $h\nu$ is the photon energy, and A is a constant. By plotting $(\alpha h\nu)^2$ versus $h\nu$, the linear region of the curve is extrapolated to intersect the energy axis ($(\alpha h\nu)^2=0$) to determine the direct band gap.

In addition, the indirect band gap of the nanocomposite was evaluated using the modified Tauc relation:

$$(\alpha h\nu)^{1/2} = B(h\nu - Eg) \quad (3)$$

Where $(\alpha h\nu)1/2$ is plotted as a function of photon energy ($h\nu$), and B is a constant. The linear extrapolation of the plot to the energy axis gives the value of the indirect band gap (Eg).

As shown in Fig. 4 (A), the Tauc plot reveals a distinct linear portion in the high-energy region. Extrapolation of this region yields a direct optical band gap of approximately 3.7 eV for the nanocomposite.

This relatively wide band gap reflects the strong electronic interactions and quantum confinement effects resulting from the incorporation of Fe_3O_4, GO, and ZrO_2 within the PANI matrix. The wide gap also implies potential for the material in UV-blocking, photocatalysis, or optoelectronic applications requiring high optical thresholds.

As illustrated in Fig. 4 (B), the Tauc plot for the indirect transition displays a linear region in the lower energy range. The extrapolation of this linear region to the x-axis reveals an indirect band gap value of approximately 1.5 eV.

This lower indirect band gap suggests the presence of sub-band states and defect-induced transitions, which are typical in complex nanocomposite systems. Such features can be beneficial in applications like photocatalysis or broad-spectrum light harvesting, where extended absorption into the visible or near-infrared regions is advantageous.

Fig. 5(A) shows the plot of $(\alpha h\nu)^2$ versus photon energy (eV), which is used to estimate the direct band gap (Eg). The linear portion of the curve extrapolated to the photon energy axis

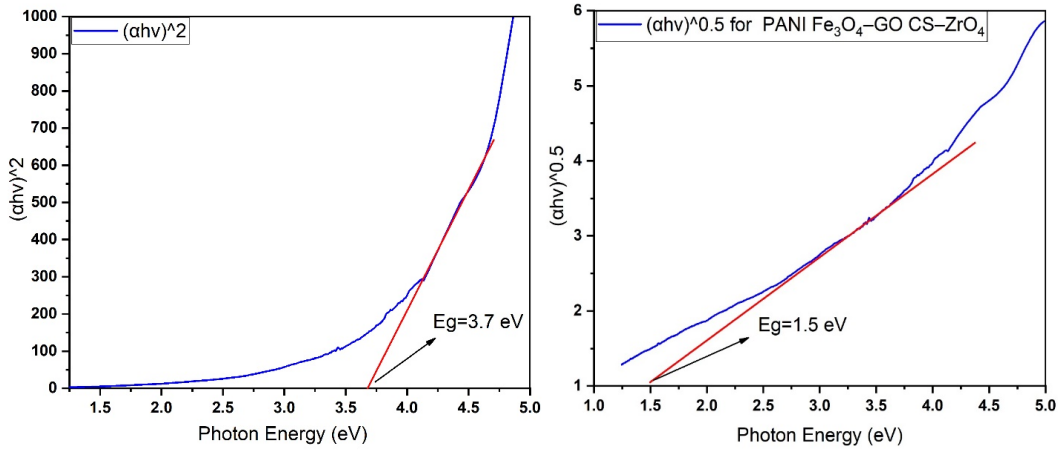

Fig. 4. A) Direct band gap for PANI/Fe_3O_4–GO/CS–ZrO_2 nanocomposite. B) Indirect band gap for PANI/Fe_3O_4–GO/CS–ZrO_2 nanocomposite.

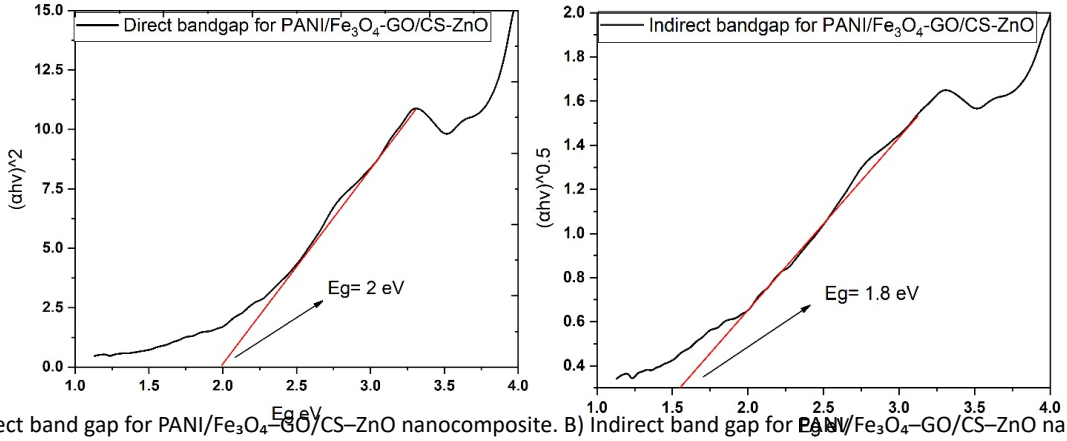

Fig. 5. A) Direct band gap for PANI/Fe_3O_4–GO/CS–ZnO nanocomposite. B) Indirect band gap for PANI/Fe_3O_4–GO/CS–ZnO nanocomposite.

gives an optical direct band gap value of approximately 2.0 eV. This relatively low band gap suggests efficient light absorption in the visible range, making the material promising for photo-induced applications such as photocatalysis and photovoltaic devices.

Fig. 5(B) illustrates the Tauc plot for the indirect transition, $(\alpha h\nu)^{1/2}$versus photon energy. The extrapolated linear portion intersects the energy axis at 1.8 eV, indicating the presence of an indirect band gap. This dual presence of direct and indirect transitions highlights the hybrid electronic structure of the nanocomposite, attributed to the synergistic interaction between the polyaniline matrix, graphene oxide sheets, and the semiconductor nanoparticles (Fe_3O_4 and ZnO).

The optical band gap values obtained for the quaternary nanocomposites indicate a clear synergistic effect arising from the integration of conducting polymer, carbon-based material, magnetic nanoparticles, and metal oxides within a single hybrid system. Pristine ZnO typically exhibits a wide band gap of approximately 3.2 eV, while ZrO_2 possesses an even wider band gap exceeding 4.0 eV. Polyaniline, on the other hand, shows variable optical transitions depending on its oxidation state and protonation level.

In the present work, the reduced effective band gap values observed for the PANI/Fe_3O_4–GO/CS–ZnO and PANI/Fe_3O_4–GO/CS–ZrO_2 nanocomposites suggest the formation of interfacial electronic states and heterojunctions between the polymeric and inorganic phases. The presence of graphene oxide facilitates charge transfer and suppresses electron–hole recombination, while Fe_3O_4 contributes additional electronic states near the conduction band.

This synergistic interaction extends light absorption into the visible region and enhances photo-induced charge separation, which directly supports the improved photocatalytic performance observed during methylene blue degradation. Similar band gap narrowing and hybrid electronic behavior have been reported in polymer/metal oxide/graphene-based nanocomposites, confirming the validity of the proposed mechanism.

Such hybrid optical behaviour enhances charge separation and prolongs carrier lifetimes, which is advantageous for improving the efficiency of photoactive materials used in environmental and energy-related technologies.

XRD Analysis of PANI/Fe_3O_4–GO/CS–ZrO_2 Nanocomposite

The X-ray diffraction (XRD) pattern of the synthesized PANI/Fe_3O_4–GO/CS–ZrO_2 nanocomposite is presented in Fig. 6. The diffraction peaks were carefully examined and indexed to identify the crystalline phases present in the nanocomposite structure.

The XRD pattern shows both sharp and broad peaks, indicating a hybrid structure comprising crystalline and semi-crystalline components. Notably, the characteristic peaks of Fe_3O_4 (magnetite) are observed at 2θ values of approximately 30.1°, 35.5°, 44.1°, 50.5°, and 60.1°. These peaks correspond to the (220), (311), (400), (422), and (440) crystallographic planes of Fe_3O_4, respectively, and are consistent with the standard JCPDS card no. 19-0629 [16].

A broad hump centered on 24.5° is attributed to the presence of amorphous graphene oxide (GO) and the semi-crystalline structure of polyaniline (PANI), a signature feature in similar nanocomposite systems [17].

Additional peaks appear at around 63° and 74.6°, which can be indexed to the (103) and (224) planes of tetragonal

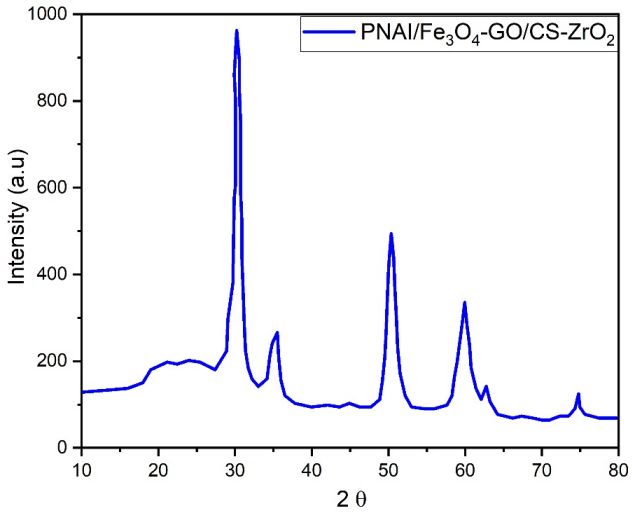

Fig. 6. The X-ray diffraction (XRD) pattern for PANI/Fe_3O_4–GO/CS– ZrO_2 nanocomposite

J Water Environ Nanotechnol, 2026, 11(3): 405-419
10.22090/jwent.2025.2076178.1992

Table 1. XRD Peak Positions and Assigned (hkl) Planes for PANI/Fe_3O_4–GO/CS–ZrO_2 Nanocomposite

2θ (°)	Phase	Assigned (hkl)	Reference
~18.3	Fe_3O_4	(111)	JCPDS 19-0629 [16]
~24.5	GO/PANI	Amorphous hump	Literature [2]
~30.1	Fe_3O_4	(220)	JCPDS 19-0629 [16]
~35.5	Fe_3O_4	(311)	JCPDS 19-0629 [16]
~43.1	Fe_3O_4	(400)	JCPDS 19-0629 [16]
~50.5	Fe_3O_4	(422)	JCPDS 19-0629 [16]
~60.1	Fe_3O_4/ZrO_2	(440)/(211)	JCPDS 19-0629, 81-1544 [16,18]
~63	ZrO_2 (T)	(103)	JCPDS 81-1544 [18]
~74.6	ZrO_2 (M)	(224)	JCPDS 81-1544 [18]

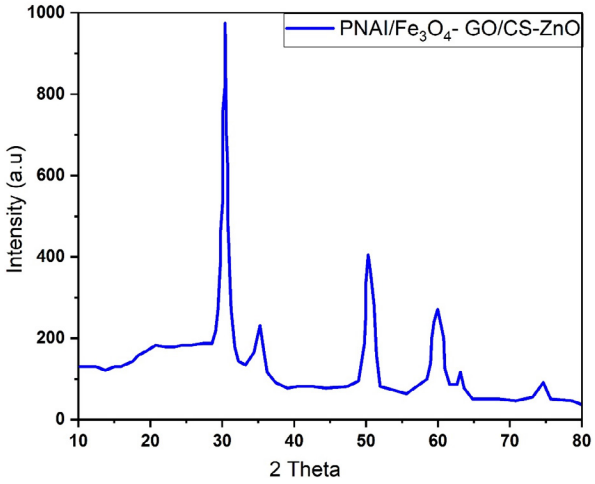

Fig. 7. The X-ray diffraction (XRD) pattern for PANI/Fe_3O_4–GO/CS–ZnO nanocomposite

and monoclinic ZrO_2, respectively, as per JCPDS card no. 81-1544 [18]. The presence of these peaks confirms the successful incorporation of ZrO_2 into the nanocomposite matrix.

The peak positions and corresponding Miller indices (hkl) are listed in Table 1. These results verify the successful synthesis of a multiphase nanocomposite consisting of Fe_3O_4, ZrO_2, GO, and PANI, with significant crystallinity and phase purity.

The X-ray diffraction (XRD) pattern of the PANI/Fe_3O_4–GO/CS–ZnO nanocomposite displays distinct peaks at specific 2θ positions that confirm the successful incorporation of all components within the composite matrix, as shown in Fig. 7.

A broad peak between 22°–26° corresponds to the (002) reflection of graphene oxide (GO), indicating disordered stacking of the graphene layers with partially retained oxygen functionalities. This broadness is typical for GO and reflects its turbostratic nature [19]. The sharp diffraction peak at ~30° is indexed to the (220) plane of Fe_3O_4, while the peak at 35.5° is assigned to the (311) plane, both consistent with the standard spinel structure of magnetite (JCPDS No. 19-0629) [16]. A diffraction peak at ~50° is attributed to the (422) plane of Fe_3O_4, confirming its crystalline phase. The peak at ~59° can be assigned to the (511) plane, and ~62.6° corresponds to the (440) plane of Fe_3O_4 as well [16]. The appearance of a peak near 74° may be attributed to a minor contribution from the (533) reflection of Fe_3O_4 or overlapping with ZnO planes (e.g., (112)) in its wurtzite structure, consistent with JCPDS No. 36-1451 [20].

The absence of sharp peaks from polyaniline (PANI) is expected, as it is semi-crystalline or amorphous. Its presence is instead inferred from background modifications and interaction with metal oxide nanoparticles, which influence peak intensities and shapes [21].

These findings confirm the co-existence of Fe_3O_4, GO, ZnO, and PANI in a hybrid nanocomposite with both crystalline and amorphous domains, suitable for multifunctional applications such as catalysis, sensing, and energy devices.

The peak positions and corresponding Miller indices (hkl) are listed in Table 2. These results verify the successful synthesis of a multiphase nanocomposite consisting of Fe_3O_4, ZnO, GO, and PANI, with significant crystallinity and phase purity.

The average crystallite size of the crystalline phases in the synthesized nanocomposites was estimated using the Scherrer

equation:

$$D = K\frac{\lambda}{\beta cos\theta}$$

where D is the crystallite size, K is the shape factor (0.9), λ is the X-ray wavelength of Cu Kα radiation (1.5406 Å), β is the full width at half maximum (FWHM) of the diffraction peak in radians, and θ is the Bragg angle.

The calculation was performed using the most intense Fe_3O_4 diffraction peak corresponding to the (311) plane at 2θ ≈ 35.5°. The estimated crystallite size was found to be approximately 20 nm for the PANI/Fe_3O_4–GO/CS–ZrO_2 nanocomposite and 25 nm for the PANI/Fe_3O_4–GO/CS–ZnO nanocomposite.

The obtained nanoscale crystallite sizes indicate that the Fe_3O_4 phase retained its nanocrystalline nature after hybridization with GO, chitosan, polyaniline, and metal oxides. The slight peak broadening observed in the composite patterns compared to pristine Fe_3O_4 suggests strong interfacial interactions and partial lattice distortion induced by polymer encapsulation and heterojunction formation. This reduction in crystallite size and peak broadening is commonly observed in multi-component polymer–oxide nanocomposites and is attributed to restricted crystal growth and increased interfacial strain.

The SEM images of the synthesized PANI/Fe_3O_4–GO/CS–ZrO_2 nanocomposite at different magnifications are presented in Fig. 8. The surface morphology appears rough and porous, with visible agglomerates of nanoscale particles forming irregular clusters. This morphology is indicative of the successful integration of polyaniline (PANI), graphene oxide (GO), iron oxide (Fe_3O_4), and zirconium dioxide (ZrO_2) within the composite matrix.

In Fig. 8(A), a layered, sponge-like structure is evident, suggesting a high surface area, which is advantageous for adsorption and photocatalytic activity. The morphology reflects the characteristic granular texture of PANI and the wrinkled sheets of GO, supporting their successful incorporation.

In Fig. 8(B), the image shows a more generalized distribution of the agglomerated particles. The particles range between 50–

Table 2. XRD Peak Positions and Assigned (hkl) Planes for PANI/Fe_3O_4–GO/CS–ZnO Nanocomposite

2θ (°)	Assigned Phase	Plane (hkl)	JCPDS Reference
22–26	GO	(002)	[1]
~30	Fe_3O_4	(220)	JCPDS 19-0629
~35.5	Fe_3O_4	(311)	JCPDS 19-0629
~50	Fe_3O_4	(422)	JCPDS 19-0629
~59	Fe_3O_4	(511)	JCPDS 19-0629
~62.6	Fe_3O_4 / ZnO	(440) / (103)	JCPDS 19-0629 / 36-1451
~74	Fe_3O_4 / ZnO	(533) / (112)	JCPDS 19-0629 / 36-1451

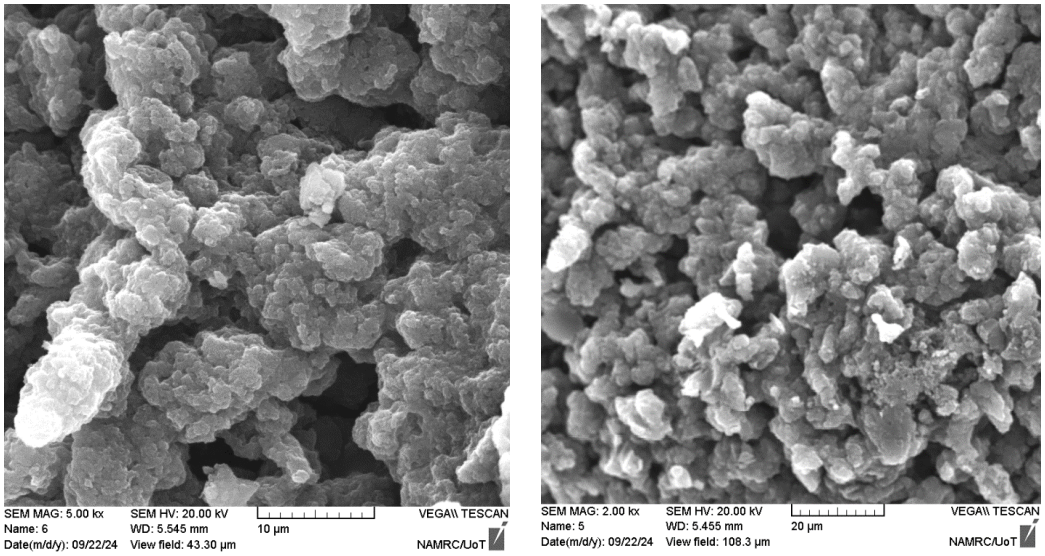

Fig. 8. SEM images of the synthesized PANI/Fe_3O_4–GO/CS–ZrO_2 nanocomposite (A) (magnification: 5.00k×, scale bar: 10 µm), (B) (magnification: 2.00k×, scale bar: 20 µm)

J Water Environ Nanotechnol, 2026, 11(3): 405-419
10.22090/jwent.2025.2076178.1992

200 nm in size, while some aggregates exceed this range due to the inherent magnetic interactions and surface energy-driven clustering of Fe_3O_4 nanoparticles. Quantitative particle size analysis was performed using ImageJ software by measuring at least 50 representative particles from different SEM micrographs, yielding an average particle size of 104 nm.

This microstructure confirms that the nanocomposite possesses high surface heterogeneity and interconnectivity among the components, which can facilitate charge transport and provide active sites for photocatalytic or adsorption applications [22.23].

The surface morphology of the synthesized PANI/Fe_3O_4–GO/CS–ZnO nanocomposite was investigated using scanning electron microscopy (SEM), as shown in Fig. 9. The SEM micrographs reveal a heterogeneous and porous structure, characterized by interlinked graphene oxide (GO) sheets decorated with uniformly distributed ZnO nanorods and Fe_3O_4 nanoparticles. The GO appears as wrinkled and layered sheets, providing a high surface area platform for the deposition of other components. ZnO nanorods, distinguishable by their rod-like shapes, are dispersed across the GO surface and embedded within the polyaniline (PANI) matrix. These nanorods are essential for enhancing charge separation and light scattering properties [24].

The Fe_3O_4 nanoparticles, appearing as quasi-spherical particles, are integrated within the composite, likely anchored onto the GO sheets and surrounded by the conductive PANI chains. The presence of chitosan (CS) contributes to structural cohesion and assists in the homogeneous distribution of metal oxides through its polymeric network [25]. The porous and textured morphology observed is consistent with previous studies of multi-component nanocomposites used for photocatalysis and pollutant adsorption [26]. Quantitative particle size analysis was performed using ImageJ software by measuring at least 50 representative particles from different SEM micrographs. The particle size was found to range mainly between 50 and 200 nm, with an average particle diameter of 96 nm.

The SEM results confirm successful integration of all components into a cohesive nanocomposite, with a surface architecture favourable for photocatalytic and adsorption-based applications due to enhanced light absorption, active surface area, and interfacial charge transport pathways.

Photocatalytic Degradation of Methylene Blue

Fig. 10 (A) displays the UV–Vis absorption spectra of methylene blue (MB) at 50 ppm before and after treatment with PANI/Fe_3O_4–GO/CS–ZrO_2 (catalyst 1). The pristine MB solution exhibits a prominent absorption peak at approximately 664 nm, corresponding to the π–π^* transition of the aromatic ring structure in MB molecules [27]. Upon the addition of catalyst 1, a noticeable decrease in the peak intensity is observed after mixing, indicating partial degradation of the dye. Following 48 hours of interaction, the peak at 664 nm nearly vanishes, confirming the significant degradation efficiency of the catalyst. The gradual reduction in absorbance signifies the disruption of MB's conjugated system due to photocatalytic oxidation.

Fig. 10 (B) presents similar absorption spectra for MB degradation using PANI/Fe_3O_4–GO/CS–ZnO (catalyst 3). As with sample 1, a substantial drop in absorbance at 664 nm is recorded upon initial contact, followed by an even more pronounced decline after 48 hours, suggesting that both

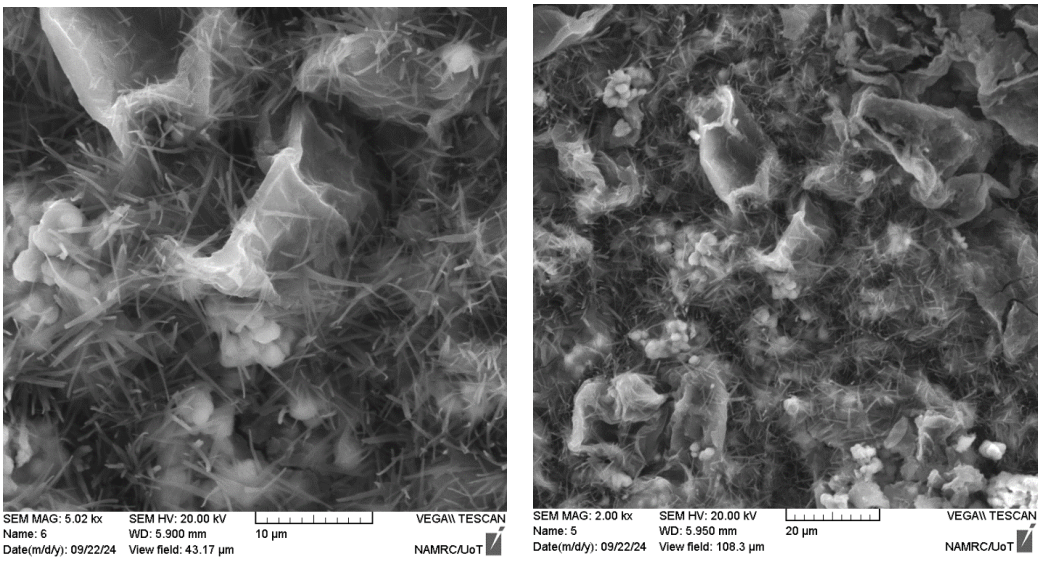

Fig. 9. SEM images of the synthesized PANI/Fe_3O_4–GO/CS–ZnO nanocomposite (A) (magnification: 5.00k×, scale bar: 10 µm), (B) (magnification: 2.00k×, scale bar: 20 µm),

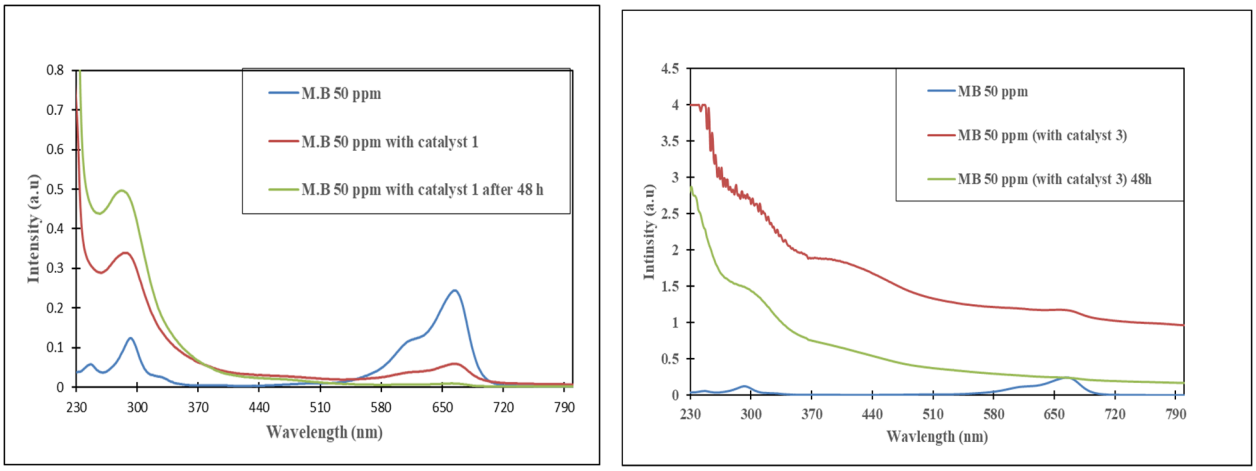

Fig. 10. (A) displays the UV–Vis absorption spectra of methylene blue (MB) at 50 ppm before and after treatment with PANI/Fe_3O_4–GO/CS–ZrO_2 (catalyst 1). (B) PANI/Fe_3O_4–GO/CS–ZnO (catalyst 3).

catalysts effectively decompose MB under ambient conditions. However, catalyst 3 shows faster and more aggressive absorption suppression, especially in the early stages, which could be attributed to the enhanced surface area, light absorption, and electron–hole separation efficiency contributed by the ZnO nanoparticles [28].

Quantitative Comparison of Photocatalytic Degradation Performance

The photocatalytic degradation of methylene blue (MB, 50 ppm) was quantitatively evaluated for both quaternary nanocomposites by monitoring the absorbance intensity at 664 nm, as shown in Fig. 10(A, B). For the pristine MB solution, a strong absorption band was observed at 664 nm with an initial absorbance of approximately $A_0 \approx 0.23–0.24$.

After 48 h of treatment with PANI/Fe_3O_4–GO/CS–ZrO_2 (catalyst 1), the absorbance at 664 nm decreased to nearly $A_{48}h \approx 0.01$, corresponding to a degradation efficiency of approximately 95%. In contrast, treatment with PANI/Fe_3O_4–GO/CS–ZnO (catalyst 3) reduced the absorbance to about $A_{48}h \approx 0.03–0.04$, yielding a degradation efficiency of approximately 85% after the same irradiation period.

The degradation efficiency was calculated using the relation $(A_0 - A_t)/A_0 \times 100$, assuming a linear correlation between absorbance and concentration. The higher degradation efficiency observed for catalyst 1 suggests a more effective interaction between the ZrO_2-containing hybrid structure and MB molecules, possibly due to differences in surface adsorption behavior and interfacial charge transfer pathways. Nevertheless, both nanocomposites exhibited strong photocatalytic activity under ambient laboratory light conditions, as evidenced by the substantial suppression of the characteristic MB absorption band.

Figs. 11, 12, and 13 illustrate the preparation of methylene blue (MB) solutions at varying concentrations, beginning with 50 ppm. The images clearly demonstrate the progressive decolorization of MB at 50, 100, and 200 ppm following treatment with the synthesized PANI/Fe_3O_4–GO/CS–ZrO_2 nanocomposite (catalyst 1). Similarly, the fading of the characteristic blue color of MB is observed after treatment with PANI/Fe_3O_4–GO/CS–ZnO (catalyst 3), indicating effective dye degradation across all tested concentrations. This visual evidence supports the photocatalytic efficiency of both nanocomposites in breaking down MB under the applied conditions.

These results indicate that the synthesized nanocomposites act as efficient photocatalysts under light exposure, likely due to synergistic effects among PANI (conductive polymer), Fe_3O_4 (magnetic core), GO (electron mediator), and metal oxides (ZrO_2 or ZnO). The combination promotes strong light harvesting, charge transport, and reactive oxygen species (ROS) formation, leading to the breakdown of organic dye molecules in aqueous media. This demonstrates the potential of such hybrid nanostructures for wastewater treatment applications.

Heavy Metal Ion Removal Performance by ICP-OES

The heavy metal ion removal efficiency of the synthesized nanocomposites was evaluated using inductively coupled plasma optical emission spectroscopy (ICP-OES), focusing on the removal of cadmium (Cd), chromium (Cr), and nickel (Ni) ions from aqueous solutions. Both nanocomposites—Sample 1 (PANI/Fe_3O_4–GO/CS–ZrO_2) and Sample 3 (PANI/Fe_3O_4–GO/CS–ZnO)—demonstrated significant capability in reducing heavy metal concentrations from their initial levels, as shown in Table 3.

The removal performance of Cd^{2+}, Cr^{6+}, and Ni^{2+} ions by

J Water Environ Nanotechnol, 2026, 11(3): 405-419
10.22090/jwent.2025.2076178.1992

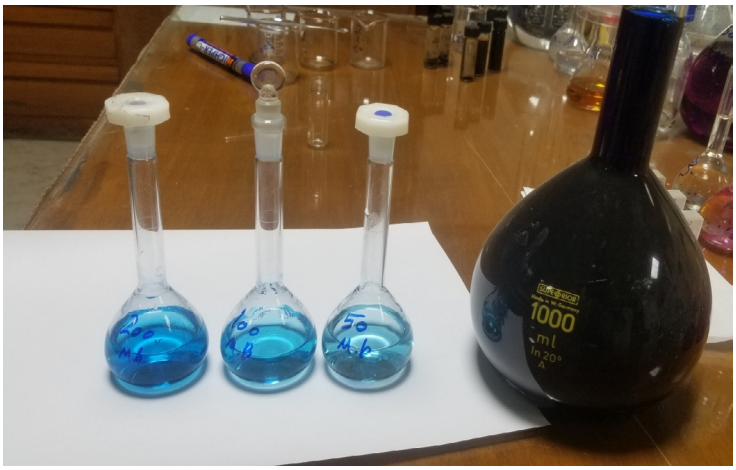

Fig. 11. Preparing different concentrations of methylene blue (MB) at 50 ppm

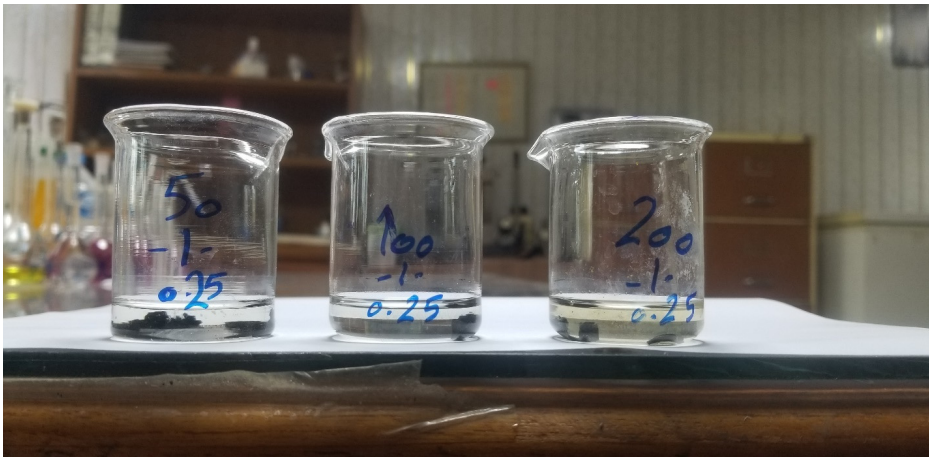

Fig. 12. shows the colour disappearance of methylene blue (MB) at 50, 100, 200 ppm after treatment with PANI/Fe_3O_4–GO/CS–ZrO_2 (catalyst 1).

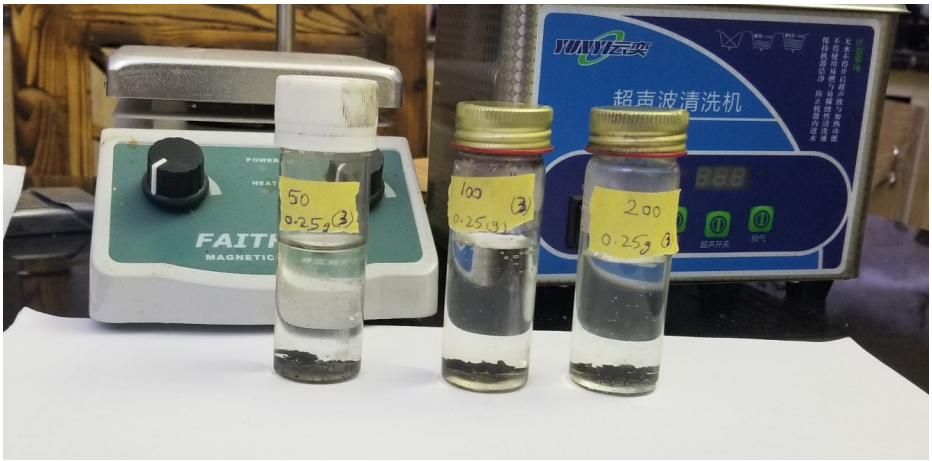

Fig. 13. shows the colour disappearance of methylene blue dye (MB) at 50, 100, 200 ppm after treatment with PANI/Fe_3O_4–GO/CS–ZnO (catalyst 3).

Table 3. ICP-OES Analysis of Cd, Cr, and Ni Removal by Nanocomposite Samples

Sample	Cd (mg/L)	Cr (mg/L)	Ni (mg/L)
Blank	0.00	0.00	0.00
Standard	2.00	1.00	1.00
Sample 1	0.24	0.65	0.57
Sample 3	0.22	1.12	0.75

Sample 1: PANI/Fe_3O_4–GO/CS–ZrO_2
Sample 3: PANI/Fe_3O_4–GO/CS–ZnO

Table 4. Comparison of the present work with similar reported nanocomposites for wastewater treatment

Material system	Target pollutant	Performance	Magnetic recovery	Reference
PANI/GO/Fe_3O_4	MB dye	~80–90% degradation	Yes	[8]
GO/CS/ZnO	MB dye	~70–85% degradation	No	[25]
GO/CS/ZrO_2	Heavy metals	~60–75% removal	No	[10]
PANI/Fe_3O_4–GO/CS–ZrO_2	MB + Cd^{2+}/Cr^{6+}/Ni^{2+}	95% MB, up to 88% metal removal	Yes	This work
PANI/Fe_3O_4–GO/CS–ZnO	MB + Cd^{2+}/Ni^{2+}	85% MB, up to 89% Cd^{2+}	Yes	This work

the synthesized quaternary nanocomposites was quantitatively evaluated using ICP-OES analysis, and the results are summarized in Table 3. The initial concentrations of Cd^{2+}, Cr^{6+}, and Ni^{2+} were 2.00, 1.00, and 1.00 mg/L, respectively.

For the PANI/Fe_3O_4–GO/CS–ZrO_2 nanocomposite (Sample 1), the residual concentrations were reduced to 0.24 mg/L for Cd^{2+}, 0.65 mg/L for Cr^{6+}, and 0.57 mg/L for Ni^{2+}, corresponding to removal efficiencies of approximately 88.0%, 35.0%, and 43.0%, respectively. These results indicate a relatively balanced adsorption behavior toward all three metal ions, with a notably higher affinity toward Cr^{6+} and Ni^{2+} compared to the ZnO-based system.

In contrast, the PANI/Fe_3O_4–GO/CS–ZnO nanocomposite (Sample 3) reduced the Cd^{2+} concentration to 0.22 mg/L, achieving a removal efficiency of approximately 89.0%, which is comparable to that of Sample 1. However, lower removal efficiencies were observed for Ni^{2+} (approximately 25.0%), while the Cr^{6+} concentration showed no effective reduction under the same conditions, suggesting weaker interaction between Cr^{6+} species and the ZnO-containing composite.

The observed selectivity differences between the two nanocomposites can be attributed to the surface chemistry of the metal oxide components. ZrO_2 possesses a higher density of surface hydroxyl groups and stronger affinity toward oxyanion species such as Cr^{6+}, enhancing adsorption through ligand exchange and electrostatic interactions. Conversely, ZnO-based composites exhibit stronger interaction with divalent cations such as Cd^{2+}, resulting in higher Cd^{2+} removal efficiency.

Finally, both nanocomposites demonstrate effective heavy metal removal capability, with the ZrO_2-based system showing superior performance for Cr^{6+} and Ni^{2+}, while the ZnO-based system exhibits slightly higher selectivity toward Cd^{2+}. These results confirm that the choice of metal oxide plays a critical role in tuning adsorption selectivity in multifunctional quaternary nanocomposites.

Comparison with Previously Reported Nanocomposites

Table 4 compares the performance of the present quaternary nanocomposites with previously reported binary and ternary systems used for wastewater treatment. Most reported materials focus on either dye degradation or heavy metal adsorption, whereas the current quaternary systems demonstrate dual functionality within a single platform.

The integration of polyaniline and graphene oxide provides a conductive network and abundant adsorption sites, while Fe_3O_4 enables rapid magnetic separation. The incorporation of ZrO_2 or ZnO further enhances selectivity toward different pollutants, allowing tunable performance depending on the target contaminant. Compared to previously reported ternary systems, the present nanocomposites exhibit higher degradation efficiency for methylene blue and competitive heavy metal removal under ambient conditions, without requiring complex synthesis steps.

These results highlight the advantage of the quaternary design in combining photocatalytic activity, adsorption capacity, and magnetic recyclability, making the developed materials promising candidates for multifunctional wastewater treatment applications.

Reusability, Stability, and Practical Considerations

The reusability and operational stability of the synthesized quaternary nanocomposites are critical factors for their practical application in wastewater treatment. The incorporation of

J Water Environ Nanotechnol, 2026, 11(3): 405-419
10.22090/jwent.2025.2076178.1992

Fe_3O_4 nanoparticles enables efficient magnetic separation of the catalysts from aqueous media, allowing facile recovery without filtration or centrifugation. This magnetic property significantly reduces material loss and simplifies reuse in repeated treatment cycles.

The structural stability of the nanocomposites is supported by the polymeric matrix formed by polyaniline and chitosan, which provides mechanical integrity and prevents excessive leaching of metal oxide components during aqueous operation. Previous studies on similar polymer-based magnetic nanocomposites have demonstrated minimal metal leaching and stable performance over multiple cycles, suggesting that the present systems are expected to exhibit comparable stability.

Although systematic recyclability and leaching experiments were not conducted in the current study, the strong interfacial interactions among PANI, GO, Fe_3O_4, and metal oxides indicate good resistance to structural degradation. Future work will focus on repeated adsorption–photocatalysis cycles and quantitative evaluation of metal leaching to further validate long-term performance.

From a practical perspective, the synthesis route employed in this work involves low-temperature aqueous processes and commercially available precursors, which are favourable for scalability. The absence of high-pressure or high-temperature steps, combined with magnetic recoverability, enhances the economic feasibility of the proposed nanocomposites for large-scale wastewater treatment applications.

CONCLUSION

In this work, magnetic quaternary nanocomposites based on PANI/Fe_3O_4–GO/CS–ZrO_2 and PANI/Fe_3O_4–GO/CS–ZnO were successfully synthesized and evaluated for combined photocatalytic dye degradation and heavy metal adsorption. Structural and morphological analyses confirmed the formation of hybrid nanocomposites with nanoscale crystallite size and porous surface architecture, which are favorable for both adsorption and photocatalytic processes.

Photocatalytic experiments demonstrated efficient degradation of methylene blue under ambient light conditions, with the ZrO_2-based nanocomposite exhibiting higher degradation efficiency compared to the ZnO-based system. Heavy metal removal studies revealed that both nanocomposites effectively reduced Cd^{2+}, Cr^{6+}, and Ni^{2+} concentrations from aqueous solutions, with distinct selectivity depending on the incorporated metal oxide. The ZrO_2-containing composite showed enhanced affinity toward Cr^{6+} and Ni^{2+}, while the ZnO-based system displayed slightly higher selectivity for Cd^{2+}.

The integration of conductive polymers, graphene oxide, magnetic nanoparticles, and metal oxides within a single quaternary framework provides a synergistic combination of adsorption sites, photoactivity, and magnetic separability. This multifunctional design enables simultaneous treatment of mixed pollutants and facilitates catalyst recovery, supporting the potential application of these nanocomposites in practical wastewater remediation systems.

Conflict of Interest
The authors declare no conflict of interest.

Funding
This study was not supported by any funding.

Author's Contributions
Study Conception or Design: I.A.
Data Acquisition: I.A., A.A.
Data Analysis or Interpretation: I.A., A.A.
Manuscript Drafting: I.A.
Critical Manuscript Revision: A.A.
All authors have approved the final manuscript and are responsible for all aspects of the work.

AI Statement
The authors confirm that no AI tools or services were used during the preparation of this work.

Data Availability Statement
The data that support the findings of this study are available from the corresponding author upon reasonable request.

REFERENCES

1. Velusamy S, Roy A, Sundaram S, Mallick TK. A Review on Heavy Metal Ions and Containing Dyes Removal Through Graphene Oxide-Based Adsorption Strategies for Textile Wastewater Treatment. Chem Rec. 2021;21(7):1570-1610. https://doi.org/10.1002/tcr.202000153
2. Melchor-Durán AP, et al. Heavy Metal Removal from Water Using Graphene Oxide in Magnetic-Assisted Adsorption Systems: Characterization, Adsorption Properties, and Modelling. Separations. 2024;11(10):294. https://doi.org/10.3390/separations11100294
3. Zhang Y, Zhang Y, Wang Y, Wang X. Graphene oxide-based materials for efficient removal of heavy metal ions from aqueous solutions: A review. Environ Pollut. 2019;252:62-73. https://doi.org/10.1016/j.envpol.2019.05.050
4. Anegbe B, et al. Graphene oxide synthesis and applications in emerging contaminant removal: a comprehensive review. Environ Sci Eur. 2024;36(1):15. https://doi.org/10.1186/s12302-023-00814-4
5. Al-Nafiey A, et al. One step to synthesis (rGO/Ni NPs) nanocomposite and using to adsorption dyes from aqueous solution. Mater Today Proc. 2019;19(1):94-101. https://doi.org/10.1016/j.matpr.2019.07.663
6. Yaseen M, et al. Facile synthesis of Fe3O4-SiO2 nanocomposites for wastewater treatment. Macromol Mater Eng. 2023;308(7):2200695. https://doi.org/10.1002/mame.202200695
7. Adel M, et al. Removal of heavy metals and dyes from wastewater using graphene oxide-based nanomaterials: A critical review.

Environ Nanotechnol Monit Manag. 2022;18:100719. https://doi.org/10.1016/j.enmm.2022.100719
8. Maponya TC, et al. Polyaniline-Based Nanocomposites for Environmental Remediation. In: Heavy Metal Ions Removal. IntechOpen; 2019.
9. Kyzas GZ, et al. Magnetic graphene oxide: effect of preparation route on reactive black 5 adsorption. Materials (Basel). 2013;6(4):1360-1376. https://doi.org/10.3390/ma6041360
10. Thabet AA, et al. Synthesis and characterization of chitosan/zro2 nanocomposite and its application in the removal of rose Bengal dye. Egypt J Chem. 2022;65(12):357-367. https://doi.org/10.21608/ejchem.2022.120576.5408
11. Sahoo SK, Rana D, Nayak A. A review on spectroscopic studies of polyaniline and its composites. Mater Today Proc. 2021;44:2096-2100.
12. Wang Y, et al. Graphene oxide covalently grafted polyaniline nanocomposite for supercapacitor: Effect of polymerization methods. Electrochim Acta. 2016;222:1763-1773.
13. Bhachu DS, et al. Compositional dependence of optical properties in Fe_3O_4-ZrO_2 nanocomposites. J Phys Chem C. 2012;116(38):20244-20252.
14. Sharma S, Tiwari A. Photocatalytic and photothermal materials based on polyaniline and metal oxides. Prog Org Coat. 2020;147:105872.
15. Shinde SM, Bhagat MD, Patil VB. Polyaniline/ZnO nanocomposites for efficient photocatalytic degradation of dyes under UV irradiation. Appl Surf Sci. 2015;347:208-216.
16. JCPDS Card No. 19-0629, Magnetite (Fe_3O_4). International Centre for Diffraction Data; 1999.
17. Xu Z, et al. Graphene oxide-based adsorbents for removal of heavy metal ions: A review. J Environ Manage. 2017;187:147-162.
18. Al-Suhaibani MS, et al. Hybrid polyaniline-metal oxide nanocomposites: Morphology and functional performance. J Mater Sci Mater Electron. 2020;31(11):8910-8924.
19. Ferrari AC, Basko DM. Raman spectroscopy as a versatile tool for studying the properties of graphene. Nat Nanotechnol. 2013;8(4):235-246. https://doi.org/10.1038/nnano.2013.46
20. JCPDS Card No. 36-1451, Zinc Oxide (ZnO). International Centre for Diffraction Data; 2001.
21. Stejskal M, Gilbert RG. Polyaniline. Preparation of a conducting polymer. Pure Appl Chem. 2002;74(5):857-867. https://doi.org/10.1351/pac200274050857
22. Kandimalla PB, Boddula RV. Synthesis and characterization of GO-metal oxide hybrid nanostructures for catalytic and sensing applications. J Mol Liq. 2020;305:112845.
23. Zhang H, Chen G, Bahnemann DW. Photoelectrocatalytic materials for environmental applications. J Mater Chem. 2009;19(29):5089-5121. https://doi.org/10.1039/b821991e
24. Reetz MT, et al. Entrapment of Nanoparticles in Polymer Matrices: A New Approach to Stable Catalysts. Adv Mater. 2004;16(22):2114-2117.
25. Kumar S, Kumar A, Sharma S. Fabrication of ZnO-GO and its nanocomposite with polyaniline for enhanced photocatalytic activity. J Alloys Compd. 2020;815:152357.
26. Rauf MA, Meetani MA, Khaleel A, Hisaindee S. Photocatalytic degradation of methylene blue using a mixed catalyst and product analysis by LC/MS. Chem Eng J. 2010;157(2-3):373-378. https://doi.org/10.1016/j.cej.2009.11.017
27. Zhang Z, Wang C, Zakaria Z, Ying J. Role of particle size in nanocrystalline TiO_2-based photocatalysts. J Phys Chem B. 1998;102(52):10871-10878. https://doi.org/10.1021/jp982948+
28. Badruddoza H, Shawon M, Tay MS, Sheng Y, Hidajat K, Uddin MS. Fe_3O_4/cyclodextrin polymer nanocomposites for the removal of copper ions from aqueous solutions. Carbohydr Polym. 2012;91(1):322-332. https://doi.org/10.1016/j.carbpol.2012.08.030
29. Afkhami A, Madrakian T, Zarei AA. Removal of heavy metal ions from aqueous solutions using Fe_3O_4, MnO_2 and $MnFe_2O_4$ nanoparticles. J Hazard Mater. 2012;211-212:379-385.
30. Wang S, Peng Y. Natural zeolites as effective adsorbents in water and wastewater treatment. Chem Eng J. 2009;156(1):11-24. https://doi.org/10.1016/j.cej.2009.10.029